Statistical Considerations for Total Isotropic Sensitivity of Wireless Devices Measured in Reverberation Chambers

Robert D. Horansky, Thomas B. Meurs, Matthew V. North, Chih-Ming Wang, Maria G. Becker, Kate A. Remley

National Institute of Standards and Technology
Boulder, CO, USA
horansky@nist.gov

***Abstract*— The vast array of wireless device form factors being developed for internet-of-things applications necessitates a flexible test environment for determining performance metrics such as total isotropic sensitivity. Reverberation chambers loaded with lossy absorbers at cellular frequencies are an ideal match for this need. However, the estimate of total isotropic sensitivity from measurements in the reverberation chamber depends on the amount of loading in the chamber and on the choice of statistical averaging used in the measurements. We present results showing the significance of these two variables.**

Keywords—cellular devices; internet-of-things; over-the-air test; wireless systems; total isotropic sensitivity

I. INTRODUCTION

There will be more mobile-connected devices than people on the Earth by the year 2019 [1]. The largest number of these devices are supporting machine-to-machine (M2M) and internet-of-things (IoT) applications with no human interaction. Unlike smartphones, M2M and IoT devices take on a vast array of small and large form factors necessitating flexibility in a test environment. Cellular devices often have integrated antennas ruling out the use of conducted measurements so that over-the-air (OTA) techniques are needed. Some key metrics for network system performance of a device do not need angle-of-arrival information, such as total isotropic sensitivity (TIS) of the receiver, data throughput, and total radiated power (TRP). Reverberation chambers are a flexible solution for these averaged system-level metrics, giving users the ability to place a device-under-test (DUT) almost anywhere in the large working volume and providing relatively low cost of construction when compared to anechoic chambers [2-6].

The reverberation chamber is an electrically large, resonating cavity. The chamber utilizes various stirring mechanisms, traditionally asymmetric rotating paddles, that allow the boundary conditions to be altered sufficiently to mix many electrical modes. The mode mixing yields, on average, a uniform electric field distribution over a large volume of the chamber. The highly resonant, mixed environment is good for providing uniformity of the electric field, but it also has the effect of creating large fluctuations in the chamber transfer function as a function of frequency. In an unloaded chamber, the frequency selectivity of the channel is typically too high for a wireless device's receiver to correct with equalization and prevents a successful communication link. Therefore, the chamber is loaded with RF absorber to decrease the quality factor of the chamber and flatten the frequency response enough to allow communication between a base station simulator and the device under test [2]. Insufficient loading of the chamber, however, can have a large impact on metrics where the quality of the communication link is being measured, such as TIS [7].

The TIS of a wireless device is normally calculated based on two separate measurements. The first determines the power transfer function of the chamber configuration averaged over many boundary conditions, which is an estimate of the loss in the channel the DUT is experiencing. This measurement is typically done as a pre-characterization of the chamber to determine how much loading the chamber requires to flatten the frequency response sufficiently for the given communication link [7]. The second measurement, also averaged over boundary conditions, determines the proficiency with which the device can demodulate a received signal for a given transmitter power. This measurement is typically performed quickly on customer provided DUTs and combined with the previously measured pre-characterization parameters to yield the TIS of each device. The use of reverberation chambers for testing modulated-signal receiver performance is a relatively young field [3]. There are very few articles examining the dependence of the TIS measurement itself on chamber characteristics, e.g. [2, 8].

The measurements for channel response and receiver sensitivity can be performed at different times under similar but non-identical conditions so that each must be averaged separately. The choice of statistical averaging technique affects the value and uncertainty determined for TIS. Here, we examine the dependence of the TIS estimated for a large-form-factor wireless router and its uncertainty on the choice of averaging and as a function of chamber loading. We compare measurements made with two different chamber setups. The first is a typical configuration where the channel loss and the receiver sensitivity are measured with separate antennas, and the second setup automates the chamber characterization and DUT measurement to occur almost simultaneously. The automated setup allows the instantaneous channel experienced by the DUT at each boundary condition to be measured, facilitating comparison of averaging methods.

We start, in Section II, by describing the measurements and calculations that go into the TIS metric in a reverberation chamber. Then, we describe the various measurement configurations in Section III. Section IV contains the results and analysis, while we conclude and describe future directions in Section V.

II. TOTAL ISOTROPIC SENSITIVITY (TIS)

The TIS is a metric for determining the receiver sensitivity of a wireless device averaged over all angles-of-incidence. The measurement requires establishing a communication link with a device, sending a known sequence as a preamble, and determining the minimum power necessary at the device to maintain a bit-error-rate (BER) below a given threshold. This threshold is 1.2% for WCDMA in [7]. The TIS determines the power incident on the receiver antenna, so it can be compared to conducted measurements, if possible. Therefore, the TIS measurement requires a measurement of the power emitted by a base-station simulator, P_{BSS}, and a measurement of the reverberation-chamber reference power transfer function, G_{ch}, which is a comparable quantity to the range path loss in an anechoic chamber.

The G_{ch} is measured with a measurement antenna that remains in the chamber during the tests, and a reference antenna used for determining the chamber characteristics. It is measured at N steps of a stirring sequence, which in our case is just the paddle of the chamber rotating in static, discrete steps. At each paddle location, n, G_{ch} is given by [2],

$$G_{\mathrm{ch}}(n) = \frac{\left\langle \left| S_{21}(n) \right|^2 \right\rangle_{\mathrm{F}}}{\left(1 - \left| \left\langle \left\langle S_{22} \right\rangle_F \right\rangle_N \right|^2 \right) \eta_{\mathrm{ref}}}, \tag{1}$$

where S_{21} is the forward transmission scattering parameter measured by a vector network analyzer (VNA), S_{22} is the reflection scattering parameter measured at the VNA port connected to the reference antenna, η_{ref} is the radiation efficiency of the reference antenna, and the brackets represent the ensemble average over the frequencies in the bandwidth of interest, F, and all the stirring positions, N. The efficiency and mismatch of the measurement antenna are not included in (1) since that antenna is used for both the G_{ch} and the P_{BSS}. The chamber reference power transfer function, G_{ref}, is related to (1) by including the measurement antenna terms in the denominator.

In addition to G_{ch}, we measure P_{BSS} by using the measurement antenna used in (1), but connecting it to a base station simulator which will now measure the transmit and receive communication signals. At each step of the stirring sequence, a communication link is established at a given output power from the base station simulator. A pseudorandom bit sequence is used as the data and transmitted to the DUT. The DUT transmits the received sequence back to the communication tester, and the error rate in the returned sequence is calculated and reported. The output power is then lowered and the BER is measured again. The power output resulting in the threshold BER is recorded for each stirring-sequence step, n.

If the measurements for G_{ch} and P_{BSS} were taken in precisely the same configuration at each stirring sequence step, then the TIS power, P_{TIS}, is the mean of the value at each step and is given by

$$P_{\mathrm{TIS}} = \frac{1}{N} \sum_{n=1}^{N} G_{\mathrm{ch}}(n) P_{\mathrm{BSS}}(n). \tag{2}$$

In the typical use of a reverberation chamber, G_{ch} will be characterized as a function of loading, with the absorber locations recorded, when the chamber is initially set up so that only a device measurement is necessary afterwards. Thus, G_{ch} and P_{BSS} are usually measured separately and must be averaged separately to calculate P_{TIS}. Furthermore, P_{TIS} is an intrinsic quantity of the wireless device, so G_{ch} and P_{BSS} are dependent quantities. That is, at each stirrer step if one value goes up, the other should ideally compensate. Thus, we separate the dependence in (2) as,

$$\frac{P_{\mathrm{TIS}}}{P_{\mathrm{BSS}}(n)} = G_{\mathrm{ch}}(n), \tag{3}$$

so that if the chamber response and base station power are measured with different realizations of the stir sequence, represented by N_1 and N_2, we can calculate P_{TIS} by

$$\begin{aligned} \frac{1}{N_1} \sum_{n_1=1}^{N_1} \frac{P_{\mathrm{TIS}}}{P_{\mathrm{BSS}}(n_1)} &= \frac{1}{N_2} \sum_{n_2=1}^{N_2} G_{\mathrm{ch}}(n_2), \\ P_{\mathrm{TIS}} &= \frac{N_1}{\sum_{n_1=1}^{N_1} \frac{1}{P_{\mathrm{BSS}}(n_1)}} \frac{1}{N_2} \sum_{n_2=1}^{N_2} G_{\mathrm{ch}}(n_2). \end{aligned} \tag{4}$$

Typically, N_1 and N_2 are the same stirring sequence, but with slightly different measurement configurations, such as a different reference and DUT antenna. Eqn. (4) is calculating an arithmetic mean of G_{ch} and a harmonic mean of P_{BSS}, and matches what is defined in the CTIA test plan for commercial test labs [7]. However, there is nothing unique about this choice of averaging and we could recast (2) as

$$\frac{P_{\mathrm{TIS}}}{G_{\mathrm{ch}}(n_2)} = P_{\mathrm{BSS}}(n_1), \tag{5}$$

leading to,

$$P_{\mathrm{TIS}} = \frac{N_2}{\sum_{n_2=1}^{N_2} \frac{1}{G_{\mathrm{ch}}(n_2)}} \frac{1}{N_1} \sum_{n_1=1}^{N_1} P_{\mathrm{BSS}}(n_1). \tag{6}$$

This calculation uses the harmonic mean of G_{ch} and the arithmetic mean of P_{BSS}. Finally, using the median value of both G_{ch} and P_{BSS} is equally valid (since the median of the reciprocal values is equal to the median of the values), giving rise to

$$P_{\mathrm{TIS}} = \mathrm{med}\left(P_{\mathrm{BSS}}(n_1)\right) \mathrm{med}\left(G_{\mathrm{ch}}(n_2)\right). \tag{7}$$

We will compare the ramifications of the choice of statistics for TIS calculations using (4), (6), and (7) in estimating the value as well as on uncertainty.

The uncertainty in TIS is derived from measuring Q independent realizations of the stirring sequence, comprised of N steps. Since these multiple realizations are, in practice, applied only to the G_{ch} measurements, and since G_{ch} and P_{BSS} are correlated, the relative uncertainty found for G_{ch} is typically applied to P_{TIS} [7]. However, for the measurements here, both parameters have been measured with multiple realizations of the stirring sequence. We use a significance test to determine whether the uncertainty was dominated by lack of spatial uniformity between the Q samples, or was comparable to the uncertainty contribution of the samples within the N stirring sequence steps [9]. This can vary with loading, but for the setups that will be described here, the spatial uniformity was the dominant contribution to uncertainty. Therefore, the average value of TIS is given by

$$\langle P_{TIS} \rangle_Q = \frac{1}{Q} \sum_{q=1}^{Q} P_{TIS}(q), \tag{8}$$

and the uncertainty comes from the variance over Q samples,

$$u_{P_{TIS}} = \sqrt{\frac{1}{Q(Q-1)} \sum_{q=1}^{Q} \left(P_{TIS}(q) - \langle P_{TIS} \rangle_Q \right)^2}. \tag{9}$$

III. Measurement Configuration

We used two configurations of antennas in the reverberation chamber to examine the effect of statistical averaging methods as a function of chamber loading. The first set of measurements used separate, but similar, antenna setups and placements for the measurements of G_{ch} and P_{BSS}. From these measurements, we realized that there would be a lot of information about the statistical nature of the reverberation chamber if we measured the instantaneous channel experienced by the DUT at each set of boundary conditions. Thus, the second set of measurements were performed with a relay circuit setup with a common antenna for G_{ch} and P_{BSS} measurements.

Common to both configurations is the chamber itself which has interior dimensions of 4.6 m x 3.1 m x 2.8 m. There is a single vertical paddle with a height of 2.1 m which traces a cylinder with radius 0.5 m. Our stirring sequence consists 72 paddle angles with 5 degree steps, N = 72. The angular coherence of the paddle was measured to be less than 5 degrees at the highest loading used here, meaning that we obtain independent measurements at each paddle orientation [10]. There was no antenna position stirring included in the stirring sequence to isolate the contribution of spatial uniformity in the chamber. The chamber was loaded with an increasing number of RF absorbers, each one measuring 0.60 x 0.60 x 0.09 m. The absorbers were added in a single stack, as is shown schematically in Fig. 1 and in the photographs in Fig. 2.

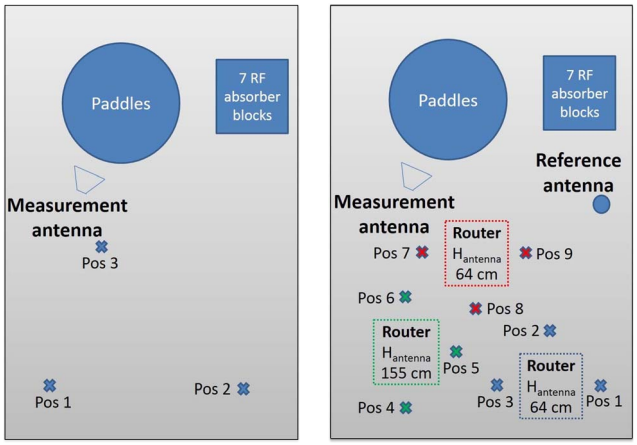

(a) G_{ref} (b) P_{BSS}

Fig. 1: Top view of the antenna positions and heights used for the measurements in the reverberation chamber. In (a) the three discone antenna positions are denoted by Pos 1 - 3 and in (b) the nine omnidirectional DUT antenna positions are denoted by Pos 1 – 9.

We performed TIS measurements using a base station simulator for a communication link in the WCDMA Band 2, Channel 9662. This is centered at 1932.4 MHz with a 3.84 MHz bandwidth. The DUT was a cellular enabled wireless router measuring 0.47 x 0.44 x 0.09 m, classifying it as a large-form-factor device [7]. An external antenna was attached to the router with a 3 m coaxial cable.

In our initial setup, the chamber transfer function, G_{ch}, and the base station output power were measured separately using different antennas for G_{ch} and P_{BSS}. For G_{ch}, the measurement antenna, which is used for both measurements, was connected to port 1 of a VNA, while the reference antenna was connected to port 2. The measurement antenna was a dual-ridge, broadband horn. The reference antenna was a discone monopole antenna. The efficiencies of the antennas were measured in the unloaded chamber [11]. We measured nine independent realizations of the stirring sequence by moving the reference antenna to three marked locations, as shown in Fig. 1(a), and at each location the reference antenna was positioned in three orthogonal polarizations. Furthermore, the independence of each stirring sequence was verified by a Pearson's correlation coefficient of less than 0.3 for all sequences [12]. We measured the chamber's power transfer function with the VNA from 1800 to 2200 MHz with 8001 points for 50 kHz steps, an IF bandwidth of 1 kHz, an output

(a) G_{ref} (b) P_{BSS}

Fig 2: Photograph of set up shown in Fig. 1 for measuring (a) G_{ch} and (b) P_{BSS}. The absorbers are shown in the back, right corner of the chamber. The measurement antenna is on the tripod on the left, the reference antenna is shown in the front of (a) and on the right in (b), and the router is shown in (b).

power of -10 dBm, and a dwell time of 10 µs. However, for calculation of (1), only a 4 MHz bandwidth around 1932.4 MHz was used.

In the initial setup, for $P_{BSS,}$ the stirring sequence was still the 72 paddle rotations, but the nine realizations of the stirring sequence were achieved by moving the router to three spatially independent locations, then rotating the router and its external antenna, as shown in Fig. 1(b). The transmit/receive port of the base station simulator was connected to the measurement antenna and the reference antenna was terminated in a 50 ohm load outside the chamber. The base station simulator power started at -60 dBm, lowered in 2 dB steps, with the BER measured at each step. When the BER exceeded 1.2%, the output power of the simulator was increased in 2 dB steps back to 0% BER, then lowered again in 0.5 dB steps until the threshold was reached and the final power recorded. If no connection was established, or the value of TIS was 30 dB or higher than the minimum value found for the stirrer sequence, the result was ignored. Fig. 2(b) shows a photograph of the router in the measurement setup for P_{BSS}. The router was placed on blocks that were measured to be transparent to RF energy at the frequencies of interest in order to keep the DUT at least 0.08 m (half a wavelength) away from the metal floor.

The configuration described above was developed according to [7]. However, it assumes that the channel corresonding to the reference measurement is, on average, the same as the channel corresponding to the DUT measurement. To understand the effects of loading on the statistics that make up the TIS metric, we designed a second setup to measure the instantaneous channel at each paddle and antenna location as well as the receiver sensitivity without touching the configuration of the chamber. The second setup consisted of a relay circuit and switch so that we can use the DUT antenna as the reference antenna as well. Fig. 3 shows a schematic of the relay system used to automate the measurement of G_{ch} and P_{BSS} with no alteration of the channel between the measurements. The stirring sequence was identical to the previous setup with the 72 stepped paddle angles, but the nine realizations of the stirring sequence were accomplished by placing the antenna on a 1 m diameter turntable and using three angular increments. A translation stage provided automated height adjustment for three heights at each turntable position.

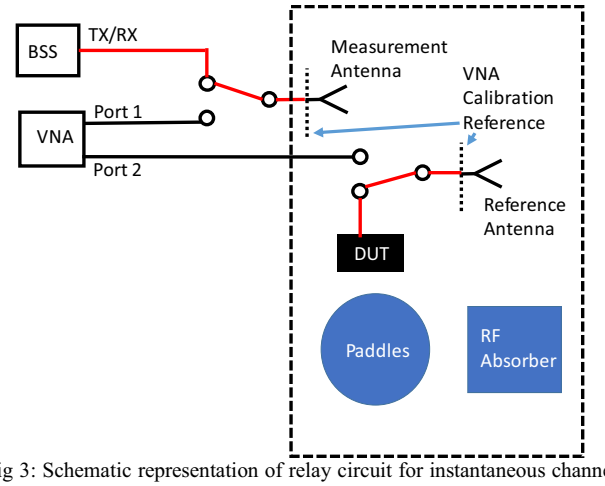

Fig 3: Schematic representation of relay circuit for instantaneous channel measurements. The dashed box represents the chamber walls. The circuit shown in red is not accounted by the calibration of the VNA measurement and that cable loss must be measured separately.

Fig. 4: Photograph of the automated setup for the reverberation chamber. The turntable has a translation stage for height adjustment and a platform with the router DUT attached by red straps.

At each location and each paddle step, the $G_{ch}(n)$ and $P_{BSS}(n)$ were measured with no change in the system except for a voltage on the relay. Chamber loss was measured with and without the relay activated to insure no effect from the presence of the relay in the chamber. A photograph of the automated setup is shown in Fig. 4.

IV. Results

We first compare our results from separate measurements of chamber response and DUT sensitivity with those taken with the automated setup. Fig. 5 shows the separated setup TIS results in red, calculated from (4), with the arithmetic mean of the chamber response and the harmonic mean of sensitivity [7]. Based on previous experience and the measurement of the frequency coherence of the chamber, the flatness of the channel was found to be good enough at seven absorbers, with the absorbers stacked sequentially in the configuration shown in Fig. 4. Once the channel has a flat enough frequency response, the average value of TIS should not change with additional loss in the chamber. Yet, with seven absorbers in the chamber, the expected plateau in TIS is observed, but is not as significant as at higher absorber loading.

The uncertainties shown in Fig. 5 for the separate measurements scenario come from determining the uncertainties of the chamber response and base-station power similarly to (9), but with the respective variable, and taking the root sum square (RSS) of the coefficients of variance, given by[13],

$$u_{P_{\mathrm{TIS}}} = \langle P_{\mathrm{TIS}} \rangle_Q \sqrt{\left(\frac{u_{P_{\mathrm{BSS}}}}{\langle P_{\mathrm{BSS}} \rangle_Q} \right)^2 + \left(\frac{u_{G_{ch}}}{\langle G_{ch} \rangle_Q} \right)^2}. \quad (10)$$

The error bars are then the standard uncertainty of P_{TIS} in dB units calculated as,

$$u\left(10\log_{10}\left(P_{\mathrm{TIS}}\right)\right) \approx 10\log_{10}\left(\frac{P_{\mathrm{TIS}} + u_{P_{\mathrm{TIS}}}}{P_{\mathrm{TIS}}} \right). \quad (11)$$

The uncertainties in Fig. 5 decrease with an increasing number of RF absorbers due to large uncertainty in the P_{BSS} term. This large uncertainty is not from lack of spatial uniformity, but rather from poorly established communication links with the DUT for channels that are highly frequency selective.

The results from the automated setup, also calculated from (4) are shown in black in Fig. 5 with excellent agreement in the overlap region of the two setups. The value of TIS does not change for seven absorbers and above indicating adequate flattening of the chamber frequency response in the communication channel, although for nine absorbers and above a distinct plateau in the mean is observed. Also, the results in the plateau region are in good agreement with anechoic chamber measurements on the same DUT which showed a P_{TIS} of 109.4 dBm. The uncertainties for the automated setup come from (9) and converted to dB with (11).

Our next analysis is to compare averaging methods for the final TIS result. In the automated setup we have access to the same instantaneous channels that the receiver measurements were performed. Thus, we can apply (2) and compare the results to those using (4), (6), and (7). Using (2), every value measured for TIS is given equivalent weighting. The harmonic mean used for (4) and (6) will tend to give more weight to lower values for P_{BSS} and G_{ch}, respectively. Finally, the median taken in (7) will unweight extreme values.

Fig. 6 shows that the choice of averaging has a large effect

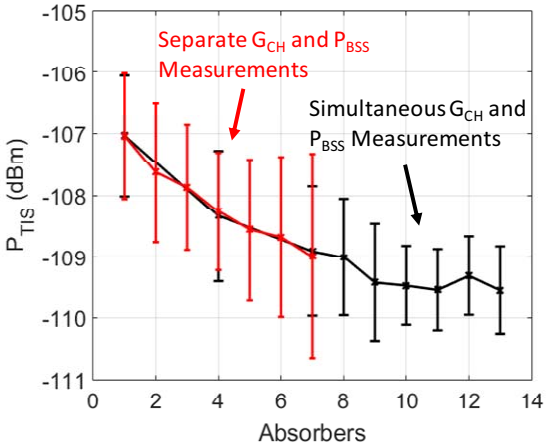

Fig. 5: Plot of TIS versus absorber loading in the chamber. The red curve is data taken with separate measurements for G_{ch} and P_{BSS}. The black curve was taken six months later using the automated setup to study the instantaneous channel. The error bars come from the lack of spatial uniformity in P_{TIS} taken from (9) for the black curve and from the RSS of the coefficient of variation in G_{ch} and P_{BSS} for the red curve.

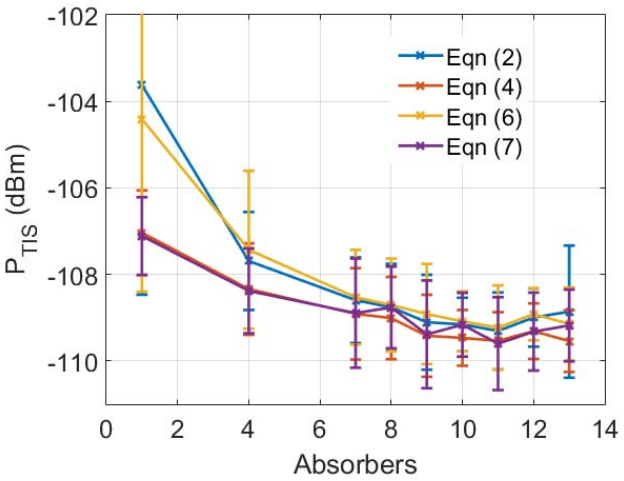

Fig. 6: Using the automated setup, plot of TIS versus absorber loading for the four averaging methods. The equation giving rise to each curve is shown in the legend. The uncertainties come from (9) .

on TIS when fewer than seven absorbers are used. However, in the plateau region with greater than eight absorbers, where the communication link is better, the averaging method is not as important. Also, in the plateau of TIS values, there is good agreement between all the methods within the uncertainty, as calculated by (9). The agreement in the plateau region leads us to conclude that the communication link is the largest contributor to uncertainty for lower absorber cases, which manifests itself as large values of $P_{\mathrm{BSS}}(n)$ when the communication link is dropped. The use of (4) and (7) tends to reduce the weight given to these higher values, leading to a more robust result. The robustness is seen in Fig. 7, which shows the relative uncertainty in P_{TIS} versus the absorber loading cases which are the error bars in Fig. 6. By using (4), as is the case in the CTIA test plan, the uncertainty in TIS is both minimized and more stable.

To verify the dominance of the uncertainty in P_{BSS}, we take a closer look at the relative uncertainty in G_{ch}. Fig. 8 shows the relative uncertainty of each of the averaging methods for G_{ch}, calculated according to (10), but with G_{ch} replacing P_{TIS}. The relative uncertainty varies only slightly at each absorber

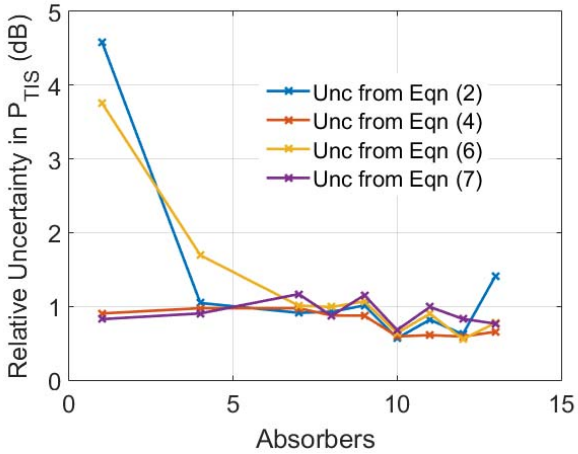

Fig. 7: The relative uncertainty due to lack of spatial uniformity in the full P_{TIS}.

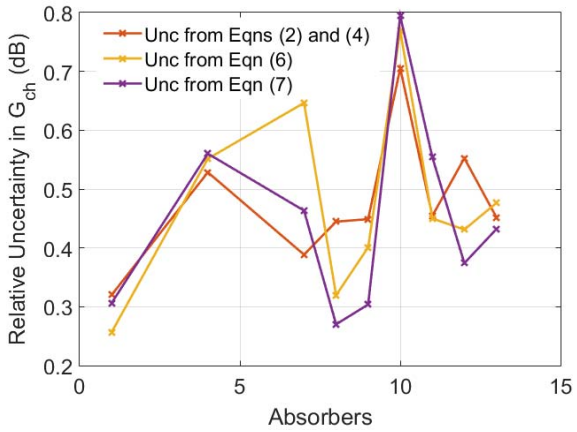

Fig. 8: The relative uncertainty considering only the lack of spatial uniformity in G_{ch} with the various averaging methods.

loading, with a generally increasing trend. The increasing trend is due to lack of spatial uniformity with increased loading [2]. Both (2) and (4) utilize the arithmetic mean for G_{ch} and are represented by the red curve. The agreement between all the curves in Fig. 7 shows that variation in G_{ch} does not depend on outliers of the measurement, even for lower absorber loading. Averaging methods that take into account the weighting of the values do not alter the results. This leads us to conclude that the uncertainty in P_{BSS} is dominated by outliers at lower absorber loading cases. Using a statistical method that reduces the weight of the high outliers in P_{BSS} such as (4) and (7) yields more relevant results for TIS.

V. Conclusion

The TIS of a wireless device is a universally utilized metric for determining its performance and requires measurement of both the link with the device as well as the channel of the measurement environment. In this paper, we presented results looking at TIS with different chamber setups and with increasing loading conditions.

With sufficient mode mixing and sampling of the chamber, the TIS of a wireless router was repeatable between two different measurement antenna setups. The first used a separate reference antenna for characterizing the chamber. The second method used a relay circuit to use the same antenna configuration for both characterizing the chamber and measuring the sensitivity of the DUT.

The relay setup allowed the instantaneous chamber characteristics at each stirrer sequence step to be known. This allowed a comparison of averaging methods. Averaging methods that reduced the weight of positive deviations in P_{BSS} were more relevant to the TIS metric, since they weight channels with stable communication links. The loaded reverberation chamber achieved good agreement with anechoic chambers with relatively small uncertainties at loading conditions that allow stable communication links. Our automated relay system allowed analysis of the effect of the instantaneous channel in the reverberation chamber on the measurement results. We then compared mathematically motivated statistical averaging choices to find the most meaningful one for TIS. Finally, the relay circuit system allows study of even more statistical metrics in the reverberation chamber. Examining the effects of various metrics in the instantaneous channel on the TIS measurement will be discussed in a future article.

Acknowledgment

We thank Edwin Mendivil at ETS-Lindgren for helpful discussion and verification of our BSS measurement procedure.

References

[1] Cisco Visual Networking Index. (2014, Feb.) Global Mobile Data Traffic Forecast Update, 2014, San Jose, CA, USA. [Online]. Available: http://www.cisco.com/c/en/us/solutions/collateral/serviceprovider/visual-networking-index-vni/white_paper_c11-520862.htm

[2] K. A. Remley, J. Dortmans, C. Weldon, R. D. Horansky, T. B. Meurs, C.-M. Wang, D. F. Williams, C. L. Holloway, and P. F. Wilson, "Configuring and Verifying Reverberation Chambers for Testing Cellular Wireless Devices," *IEEE Trans. Electromagn. Compat.,* vol. 58, no. 3, June 2016.

[3] C. Orlenius, P. S. Kildal and G. Poilasne, "Measurements of total isotropic sensitivity and average fading sensitivity of CDMA phones in reverberation chamber," *2005 IEEE Antennas and Propagation Society International Symposium*, 2005, pp. 409-412 Vol. 1A.

[4] O. Delangre, P. De Doncker, F. Horlin, M. Lienard, and P. Degauque, "Reverberation chamber environment for testing communication systems: Applications to OFDM and SC-FDE," in *Proc. 68th IEEE Veh. Technol. Conf.*, Calgary, Canada, Sept. 2008, pp. 1–5.

[5] P.-S. Kildal, C. Orlenius, and J. Carlsson, "OTA testing in multipath of antennas and wireless devices with MIMO and OFDM," *Proc. IEEE*, vol. 100, no. 7, pp. 2145–2157, Jul. 2012.

[6] C. Lötbäck Patané, A. Skårbratt, R. Rehammar, and C. Orlenius, "On the use of reverberation chambers for assessment of MIMO OTA performance of wireless devices," in *Proc. 7th Eur. Conf. Antennas Propag*., Gothenburg, Sweden, pp. 101–105, Apr. 2013.

[7] CTIA Certification, "Test Plan for Wireless Large-Form_Factor Device Over-the-Air Performance," Version Number: 1.1, July 2017.

[8] M. Andersson, C. Orlenius and P. S. Kildal, "Three Fast Ways of Measuring Receiver Sensitivity in a Reverberation Chamber," *2008 International Workshop on Antenna Technology: Small Antennas and Novel Metamaterials*, Chiba, 2008, pp. 51-54.

[9] K. A. Remley, C.-M. Wang, R. J. Pirkl, A. T. Kirk, J. Aan Den Toorn, D.F.Williams, C. L. Holloway, J. A. Jargon, and P. D. Hale, "A significance test for reverberation-chamber measurement uncertainty in total radiated power of wireless devices," *IEEE Trans. Electromagn. Compat.*, vol. 58, no. 1, pp. 207–219, Oct. 2015.

[10] R. J. Pirkl, K. A. Remley and C. S. L. Patane, "Reverberation Chamber Measurement Correlation," in *IEEE Transactions on Electromagnetic Compatibility*, vol. 54, no. 3, pp. 533-545, June 2012.

[11] C. L. Holloway, H. A. Shah, R. J. Pirkl, W. F. Young, D. A. Hill and J. Ladbury, "Reverberation Chamber Techniques for Determining the Radiation and Total Efficiency of Antennas," in *IEEE Transactions on Antennas and Propagation*, vol. 60, no. 4, pp. 1758-1770, April 2012

[12] D. F. Morrison, Multivariate Statistical Methods. New York: McGraw-Hill,1967.

[1] Joint Committee for Guides in Metrology, "Evaluation of Measurement Data-Guide to the Expression of Uncertainty in Measurement," BIPM, France, September, 2008.